Supplementary material: How to administer an antidote to Schrödinger's cat

I. SAME-DETECTOR PROBABILITIES

Fig. 3 in the main text shows the subset of probabilities when we only look at cross-detector correlations. For this reason, the value $\int P_{\text{joint}}(\tau)\, d\tau$ is bounded by 1/2. A prediction of the theoretical curves for same-detector correlations, given by $P_{\text{same}}(\tau)$ can be shown in Fig. S1. Given the different possibilities that can arise from photon routing, the normalization for the joint detection probability is given by

$$\int \left(P_{\text{joint}}(\tau) + P_{\text{same}}(\tau)\right) d\tau = 1 \tag{S1}$$

II. LATENCY OF FEEDBACK

To ensure adequate feedback, it is crucial to perform a timely change on the phase ϕ, conditional on detections only in the first time bin. However, not every detection of the SPCM can be used to change the phase of the photon: the latency between the SPCM click and the effect of the feedback electronics can affect the production of a proper photonic state which can be used for feedback. The photon signal takes around 75 ns to reach the output of the SPCMs from the EOM (as seen in the sum of the first two columns of Table S1), during which there is no possibility of achieving feedback control.

The probability of a correlation (with one detection in each time bin) occurring during the dead time is given by

$$P(\tilde{t}) = \int_{\max\left[\frac{1}{2}-\tilde{t},0\right]\delta t}^{\frac{1}{2}} f(t_1) \int_{\frac{1}{2}}^{\min\left[t_1+\tilde{t},1\right]\delta t} f(t_2)\, \mathrm{d}t_2\ \mathrm{d}t_1 \tag{S2}$$

where $\tilde{t}$ is the dead time given as a fraction of the total photon length δt, $t_1 \in \left(0, \frac{1}{2}\right)\delta t$ and $t_2 \in \left(\frac{1}{2}, 1\right)\delta t$, and

$$f(t) = \frac{16}{3}\sin^4(2\pi t/\delta t) \tag{S3}$$

is the intensity envelope of the produced photons.

The error rate remains negligibly small for dead times of up to around a fifth of the total photon length before increasing rapidly, as shown in Fig. S2. In our experiment, the control and effecting stages are implemented in 13ns, resulting in a total latency for the feedback of 97ns, corresponding to an expected error rate of 0.2%. Table S1 details the latency breakdown.

Element	Time (ns)
Optical Transit Time EOM → Cavity → SPCM	45
SPCM Response	35
Circuit Response	7.0
Signal Rise Time	5.5
Total Cable Delay SPCM → Control → EOM	4.5
Total	97.0

TABLE S1: A breakdown of the contributing elements to the feedback delay. The first two rows are not known absolutely, only their sum was measured. From discussions with the manufacturer it is believed that the SPCM response (time delay between photon impact and TTL output) is around 35 ns.

III. FAST ELECTRONICS

The task of the feedback controller is to decide whether or not a phase should be applied to the second time bin and, if so, quickly supply sufficient voltage to the electro-optic modulator to enact that phase change. To that end, a custom in-house circuit was built using off the shelf transistor-transistor logic (TTL) integrated circuit (IC) logic chips. The circuit toggles between one mode of operation with no effect and another one which ensures a phase change to the EOM during the second time bin. An abbreviated circuit logic diagram outlining the functioning of the circuit is shown in Figure S3. The control circuit receives as inputs a copy of the TTL output from the SPCM of interest, **det**, and two 215 ns TTL window pulses from the AWG, W_{det} and $\mathrm{W}_{\text{phase}}$, which respectively outline the first time bin for the registering of detections and the second time bin for the output phase voltage, **phase**.

IV. DATA PROCESSING

The data recorded by the SPCMs is processed to yield the sliding histograms and bar charts shown in Figures 3 and 4. This data contains a significant amount of noise coming from detector dark counts and other stray photons, which need to be corrected for. Five procedures are performed in the raw data after clicks are recorded in detectors C and D:

A. Gating the raw data: Correlations need to be found between the raw data. The time scale is cropped to account for photon arrival times and repumping times, which are eliminated accordingly from the scale. This is shown in Fig. S4 (a).

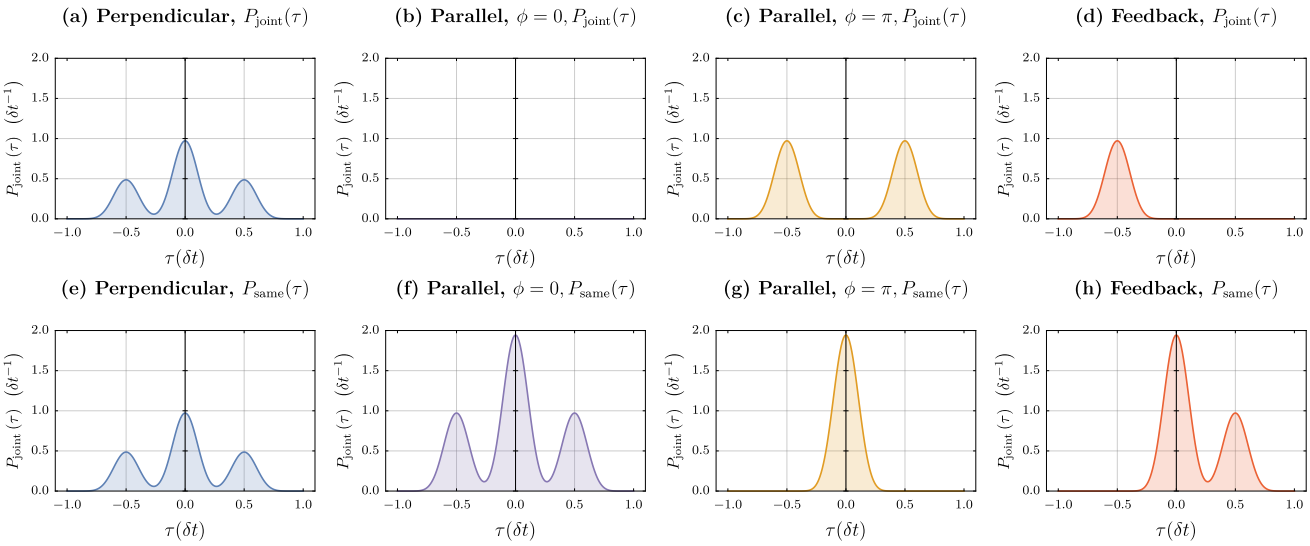

FIG. S1: Theoretical curves for $P_{\text{joint}}(\tau)$ for cross-detector (a-d) and same-detector coincidences (e-h), for the same cases described in Fig. 3 from the paper. Subfigure (f) shows that, when photons are identical, all the detections happen in the same detector, albeit possibly in different time bins. Once more, δt corresponds to the length of the single photons.

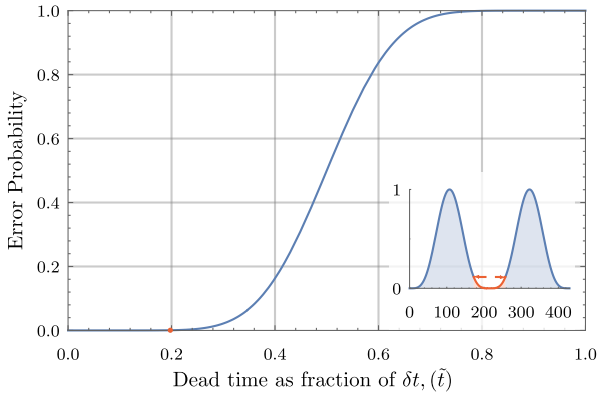

FIG. S2: Feedback error analysis: The dead time is the feedback delay of the system, here shown as a fraction of the photon length. Specifically it is the round trip time for a signal to pass from the EOM, via the cavity to the SPCMs, be processed by the controller and return to the EOM. It represents a period of time during which feedback control cannot be achieved, therefore introducing an error rate (Eq. S2). The profile of the considered photon is shown in the inset along with the measured 97 ns feedback delay of the setup marked in red, the corresponding error rate of 0.2% is coincident with the horizontal axis on this scale.

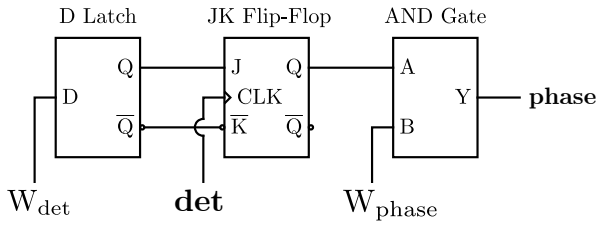

FIG. S3: Control circuit: The JK flip-flop (TI SN74F109N) controls the state of operation of the circuit. When Q is 0, no Phase signal will be output, but when Q is 1, the output, phase, follows W_{phase}, using a wired AND gate with open collector TTL gates (N74F07N). Toggling between these two states is triggered by a signal on the JK flip-flop CLK (clock) input from a detector, det, but only when the JK is in toggle mode. With Q($\overline{\text{Q}}$) high (low) the JK is in toggle mode, with Q ($\overline{\text{Q}}$) low (high) the JK is in Hold mode. The D latch (TI SN74LS375N) buffers the input W_{det} to provide a duplicated and negated copy necessary for the JK.

B. Fitting and calculation of Signal to Noise Ratio: Once the raw data has been gated, we fit the following function to the raw data in each detector:

$$g(t) = a + \begin{cases} b\sin^2\left(\frac{2\pi(x-p_1)}{p_2-p_1}\right) & \text{for } p_1 < x < p_2 \\ c & \text{for } p_3 < x < p_4 \end{cases} \quad \text{(S4)}$$

Here, p_1 and p_2 encompass the times for photon arrivals, while p_3 and p_4 correspond to times when the repumping is triggered. The time between p_2 and p_3 is used to obtain the dark count rates of the single photon counting modules. This fitting is shown in Fig. S4 (b).

C. Background estimation: A model for calculating the background is created by using the photon count and dark count rates of the single photon detectors. These rates lead to two distributions for each detector describing the detection events due to photons emitted from atoms, $m_P^{(C/D)}(t)$, and true background detections uncorrelated to atoms $m_B^{(C/D)}(t)$.

These distributions can be combined to give expected correlations between their pairwise combina-

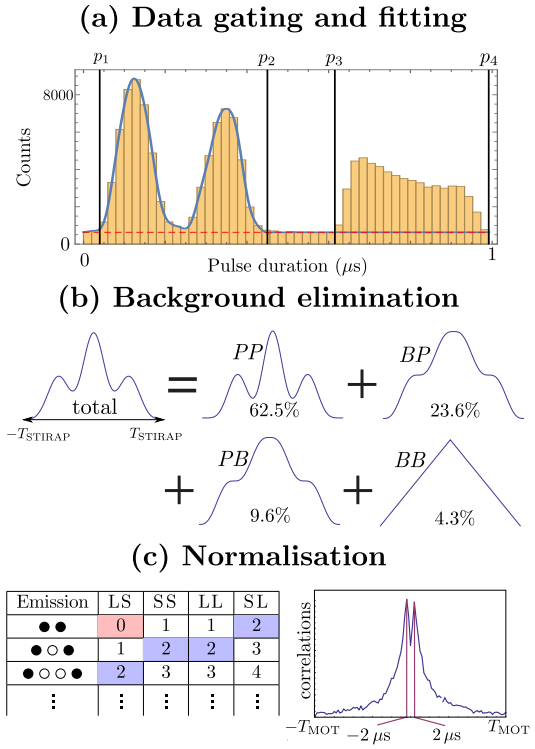

Emission	LS	SS	LL	SL
●●	0	1	1	2
●○●	1	2	2	3
●○○●	2	3	3	4
⋮	⋮	⋮	⋮	⋮

FIG. S4: Background corrections. (a) Shows the photon gating, which fits the photon shape and the repumping following Eq. S4. The photon duration begins in p_1 and ends in p_2. (b) Shows the four components of the background elimination, $M_{\mathrm{BB}}^{(C)(D)}(\tau), M_{\mathrm{BP}}^{(C)(D)}(\tau)$, $M_{\mathrm{PB}}^{(C)(D)}(\tau)$ and $M_{\mathrm{PP}}^{(C)(D)}(\tau)$. (c) shows the normalisation of the correlations. Coincident detections (red), can only occur for a sequential emission of two photons with the first photon entering the delay arm, L and the second entering the short arm S. The normalisation constant is based on the number of correlations at $\pm 2\,\mu$s in the $g^{(2)}$ (blue), for which there are four times as many pathways. Correcting for photon losses in the delay arm, we find that the normalisation factor follows Eq. S12. T_{MOT} corresponds to the time taken by an atom to be launched from the atomic fountain and fall back again, and the loss in correlations is a direct consequence of the passage of atoms through the cavity.

tions across both detectors: $M_{\mathrm{BB}}^{(C)(D)}(\tau), M_{\mathrm{BP}}^{(C)(D)}(\tau)$, $M_{\mathrm{PB}}^{(C)(D)}(\tau)$ and $M_{\mathrm{PP}}^{(C)(D)}(\tau)$, where

$$M_{\mathrm{BP}}^{(C)(D)}(\tau) = \int_0^{T_{\mathrm{STIRAP}}} m_{\mathrm{B}}^{(C)}(t) m_{\mathrm{P}}^{(D)}(t+\tau)\mathrm{d}t \quad \text{(S5)}$$

$$= \left(m_{\mathrm{B}}^{(C)} * m_{\mathrm{P}}^{(D)}\right)(\tau). \quad \text{(S6)}$$

and the other terms are defined analogously. The total background is the addition of these terms:

$$M_{\mathrm{total}}^{(C)(D)}(\tau) = M_{\mathrm{BB}}^{(C)(D)}(\tau) + M_{\mathrm{BP}}^{(C)(D)}(\tau) + M_{\mathrm{PB}}^{(C)(D)}(\tau) + M_{\mathrm{PP}}^{(C)(D)}(\tau). \quad \text{(S7)}$$

Case	Coincidence rate / noise
Fig. 3(a) - Perpendicular	2.02
Fig. 3(b) - Parallel, $\phi = 0$	0.37
Fig. 3(c) - Parallel, $\phi = \pi$	1.40
Fig. 3(d) - Parallel, feedback ϕ	0.94

TABLE S2: Integrated coincidence rate and integrated noise correction ratio of the different time-resolved HOM histograms. The noise has been eliminated from Fig. 3 in the main text.

The $M_{\mathrm{PP}}^{(C)(D)}$ term accounts for the expected correlation rate between two atoms producing photons by the distribution $m_P^{(C/D)}$, and can be discarded as we are only interested in the correlations of photons within the same emission period. A plot of the four terms composing $M_{\mathrm{total}}^{(C)(D)}(\tau)$ is shown in Fig. S4 (c). Upon removing $M_{\mathrm{total}}^{(C)(D)}(\tau)$, the ratio between the integrated coincidence rate and the integrated noise correction of the different contributions is given by Table S2.

D. Maximum likelihood estimation of correlation counts: The total number of observed correlation counts $O(\tau, \delta\tau)$ between τ and $\tau + \delta\tau$ is equal to

$$O(\tau, \delta\tau) = S(\tau, \delta\tau) + B(\tau, \delta\tau), \quad \text{(S8)}$$

i.e. the sum of signal correlation counts $S(\tau, \delta\tau)$ and background correlation counts $B(\tau, \delta\tau)$ calculated from $M_{\mathrm{total}}^{(C)(D)}(\tau)$. From $O(\tau, \delta\tau)$, we can extract the most likely mean number of signal correlation counts within such a bin with a maximum likelihood estimation. Assuming that both $S(\tau, \delta\tau)$ and $B(\tau, \delta\tau)$ follow independent Poisson distributions with parameters λ_S and λ_B, respectively, it can be shown that the probability of observing n counts equals

$$\mathrm{P}(O = n) = \frac{e^{-(\lambda_S+\lambda_B)}(\lambda_S + \lambda_B)^n}{n!}, \quad \text{(S9)}$$

i.e. $O(\tau, \delta\tau)$ follows a Poisson distribution with a mean of $\lambda_O = \lambda_S + \lambda_B$. Given an observation n for O and known λ_B (mean background), the likelihood function for the parameter $\lambda_S \in [0, \infty)$ is given by

$$\mathcal{L}(\lambda_S \mid n, \lambda_B) = \mathrm{P}_{\lambda_S}(O = n), \quad \text{(S10)}$$

which is maximised for the intuitive value of

$$\lambda_S = \max\{0, n - \lambda_B\}, \quad \text{(S11)}$$

i.e. the number of observed counts minus the background, constrained to a positive number.

E. Normalisation: Due to experimental errors in detectors, such as losses and dead times, it is not possible to identify directly how many individual photon-pair experiments were performed by counting the number of detection events measured in one detector. To

overcome this, it is possible to notice that the number of events happening simultaneous is related to the number of events happening separated by two duty cycles, following the relation

$$N_0/N_2 = \frac{\eta_L}{1 + 2\eta_L + \eta_L^2} \simeq 1/4, \tag{S12}$$

where η_L is the probability of photon transmission in the fibre delay.